Available online at www.sciencedirect.com

ScienceDirect

Procedia Computer Science 58 (2015) 18 – 25

Procedia Computer Science

Second International Symposium on Computer Vision and the Internet (VisionNet'15)

A Comparative Study of Several Array Geometries for 2D DOA Estimation

Sharareh Kiani[a,*], Amir Mansour Pezeshk[a]

[a]*Electronic Research Institute, Sharif University of Technology, Tehran, Iran*

Abstract

In this paper, a comparison between several array geometries, including planar arrays and volume arrays, for two-dimensional Direction of Arrival (DOA) estimation using Multiple Signal Classification (MUSIC) is presented. For each geometry, various criteria is taken into consideration and a comparative study of the performance of geometries is carried out. The geometries together with their ultimate direction finding performance are compared based on Root Mean Square Error (RMSE), the ambiguity functions, and Cramer-Rao Bounds (CRB). Furthermore, the effects of phase and amplitude variations of the array element radiation pattern, namely Vivaldi and Monopole antenna, on DOA estimation performance are studied. The advantages and drawbacks of each geometry vis-à-vis the employed DOA estimation technique are shown through a numerical comparison.

Peer-review under responsibility of organizing committee of the Second International Symposium on Computer Vision and the Internet (VisionNet'15)

Keywords: DOA estimation; planar array; Volume array; Ambiguity function; CRB; ESM;

1. Introduction

1.1. Motivation and Review

The application of Direction of Arrival (DOA) estimation is found in many fields, namely radar, communication, sonar, Electronic Surveillance Measure (ESM), etc. For ESM systems, the application of this paper, the DOA information of an emitter is of the utmost importance in many aspects, namely operational and de-interleaving [1].

* Corresponding author. Tel.: +98-21-66164905.
E-mail address: kiani.sh86@gmail.com

Peer-review under responsibility of organizing committee of the Second International Symposium on Computer Vision and the Internet (VisionNet'15)
doi:10.1016/j.procs.2015.08.004

Different approaches along with different array geometries have been studied in DOA estimation literatures. However, in order to attain the desired requirement of such systems, one should entertain an important caveat that the employed array geometry and the DOA estimation algorithm are both responsible for the DF system's overall performance. That is, a specific array geometry, the location of the elements in the array, imposes some theoretical bounds on the performance of different DF algorithms and gives rise to different results. Similarly, a certain DF algorithm performs differently when used with diverse array structures [3, 4].

Depending on DF algorithm, the level of accuracy and immunity to co-channel interference, multipath interference, and noise will be different [9]. For this reason, a super-resolution algorithm, namely Multiple Signal Classification (MUSIC) algorithm [2], instead of interferometry techniques [9, 10] is used. Moreover, solving ambiguities problems related to using an arbitrary geometry to an interferometer is one of the greatest impeding factors to employ such techniques. However, MUSIC is apropos to deal with different geometries. It should be noted that super-resolution techniques impose an added computational cost to the DF system in comparison with interferometry methods. Furthermore, ambiguities, a necessary performance measure, are equally important in super-resolution techniques as well. In this regard, the first-order array ambiguity function [11, 12] can be employed.

Great number of literature on DOA estimation have studied either DOA algorithms on a single array geometry or two or more geometries, evaluation of which is provided by one or two benchmarks for the performance of the geometry itself. In [3], a performance comparison on pivotal array design parameters, namely the element spacing, the number of elements, SNR (signal-to-noise ratio), and the number of samples (or snapshots) is done but only for UCA geometry. A comparison between several planar arrays ultimate capabilities is performed in [5]; however, one-dimensional Cramer-Rao Bounds (CRBs), CRB versus Azimuth angles in fixed Elevation angles, is used as the DF performance benchmark. Moreover, the elements are considered isotropic, the results of which are not completely applicable for real world situation where the elements' amplitude and phase characteristics affect the overall performance. In [6], the authors compare the circular and hexagonal geometries and impose a dipole element's phase and amplitude properties upon the arrays. The evaluation nevertheless, is apposite to Smart antenna applications in terms of applied criteria. Several high-resolution direction finding algorithms as well as possible effects of different element types are investigated in [7, 8]; the application of a circular array geometry is explored however.

1.2. Contributions

In this paper, several array geometries for joint azimuth and elevation estimation based on a super-resolution algorithm are compared. The present paper can be considered as an eclectic approach to compare geometries using an admixture of criteria presented in [3], [5], [8], and [11]. Root Mean Square Error (RMSE) of each geometry is investigated for both Horizontal and Vertical element patterns, as an accuracy criterion. We also study CRBs and the ambiguity function of every geometry that to best of our knowledge, have not been comprehensively studied together as criterion for evaluation of array geometries. We suggest several geometries, including planar and volume geometries, to be used as a part of DF equipment used in ESM applications. Circular array geometries are of especial interest by virtue of their uniform performance over the azimuth range, and being not a saturated geometry, which means they could be easily extended to a new geometry by adding elements to the structure or by changing the whole geometry into a new circular-base geometry such as a cylindrical or a spherical geometry [13].

The organization of the paper is as follows. In Section 2, the model of system as well as the scenario of our application are described. Section 3 discusses the issue of the proposed geometries and employed array elements which are Vivaldi and Monopole antennas. In Section 4, we study the CRB and the array ambiguity function of proposed geometries. Section 5 presents the simulation results and the comparison study of all geometries. And Section 6 concludes the paper.

2. System Model

2.1. Arbitrary Arrays Model

In supper-resolution direction finding algorithms, the array system model is strongly depend on the *array manifold*

[14, 15], the array properties and response to incident signals. Considering an arbitrary array consists of N elements, in an azimuth angle φ and elevation angle θ, the manifold vector *a(φ, θ)* is given by [14]:

$$a(\varphi, \theta) = g(\varphi, \theta) \odot \exp(-j \underline{r}^T k) \quad (1)$$

where $\underline{r} = [\underline{r}_x, \underline{r}_y, \underline{r}_z]^T \in R^{3\times N}$ is the array elements' position matrix with the centroid taken as (0, 0, 0), $\underline{k} = \pi[\cos\theta\cos\varphi, \cos\theta\sin\varphi, \sin\theta]^T \in R^{3\times 1}$ represents the wavenumber vector, ⊙ denotes the Hadamard product, and $g(\varphi,\theta) \in C^{N\times 1}$ is the vector of the directional gains of the array elements, including the amplitude and phase characteristics of the elements.

The array manifold is formed by the locus of all manifold vectors for the angular field of view defined in section I. Assuming M narrowband signals $s_m(t), 1 \le m \le M$ originated from different azimuth and elevation angles (φ_m, θ_m), the array output signals at time *t* is given by [15]:

$$x(t) = \sum_{m=1}^{M} a(\varphi_m, \theta_m) s_m(t) + n(t) = A(\varphi,\theta)S + N \quad (2)$$

where $A(\varphi,\theta) \in C^{N\times M}$ is the steering vector matrix, $S \in C^{M\times K}$ represents the signal matrix assuming K snapshots are collected by the array, and $N \in C^{N\times K}$ is the noise matrix, assumed to be WSS, second order ergodic, zero-mean, temporally and spatially white complex Gaussian.

With the above model, and following [2], MUSIC algorithm can be applied to the succeeding proposed geometries. As for a simple explanation of MUSIC algorithm, the received data from the elements is decomposed into the orthogonal noise subspace and signal subspace; the algorithm uses this orthogonally to estimate the direction of arrival of the incident signal. These subspaces are extracted from the eigenvalues of the covariance matrix of the received data. Finally, the azimuth and elevation estimations of incident signals are computed from the algorithm pseudo-spectrum [2].

2.2. DF Scenario

In this section a brief description of the prevailing requirements for the DF simulation scenario is provided. For the sake of high Probability of Intercept (POI), the measurement is done in an instantaneous approach [1], in which the emitter pulse is sampled throughout its waveform via several receiver channels each of which connected to one element. The receiver channels also should be able to provide both amplitude and phase measurements in order to have the potential of applying super-resolution DOA algorithms; however, in practice this would add additional costs. Due to pecuniary matters, we are allowed no more than ten receiving channel per each geometry. Therefore, two types of geometries can be employed; the first one is the geometries with at most ten elements, hereafter referred to as the *full-channel* geometries; and the second type is the geometries with more than ten elements using RF switching schemes introduced in [10], here referred to as the *switching-channel* geometries.

The first prototype of the DF system is supposed to operate in frequency range of 1 to 2 GHz, to have an estimation accuracy of Class-A according to [10], as well as to function in angular range of view of 360-degree in Azimuth and 60-degree in Elevation. In light of practical ESM application, a linear FM pulse waveform (with the pulse bandwidth=14MHz, the pulse-width=66ns and PRF=2 KHz) is simulated using MATLAB, as for the incident signal. Finally, an additive White Gaussian noise with SNR=10dB is added to the amplitudes and phases of the preceding signal.

3. Geometries and Elements

3.1. Proposed Geometries

In this section, we introduce several array geometries with different number of elements. Fig.1. shows the proposed

geometries; the arrows show the normal of the array element, namely Vivaldi antenna. The first geometry, categorized as a full-channel, is a uniform circular array (UCA) with nine element, and inter-element spacing of a half of wavelength. Without loss of generality, the number of elements is selected to be odd in order to avoid DOA ambiguities with frequencies [1]. The second geometry, which be called the *pyramid* geometry, consists of the same UCA and an extra element at the center and a half of wavelength in height. The use of the extra element is beneficial to improving the elevation estimation accuracy in that it adds some kind of vertical aperture to the geometry [13]. Likewise, the third and the forth geometries, hereafter referred to as *spiral-circular* geometry and *slanted-circular* geometry, are enjoying the benefit of vertical aperture, whereas nine elements are used. The elements of *spiral-circular* geometry gradually are elevated from the elevation level of zero degree for the first element to forty five degrees for the last element. In similar fashion, the elements in *slanted-circular* geometry are elevated up from the elevation level of zero degree to forty five degrees but until the mid-element, and again are elevated down for the rest of the elements. The next geometry is *dual-circular spherical* geometry, in which two circular arrays at two elevation levels, that is to say minus ten degrees and ten degrees, with five elements per array are configured. The last geometry, *multi-planar* geometry is categorized as *switching-channel* geometry in that it contains more than ten elements. Four planar arrays, each of which with five elements, are considered as the *multi-planar* geometry.

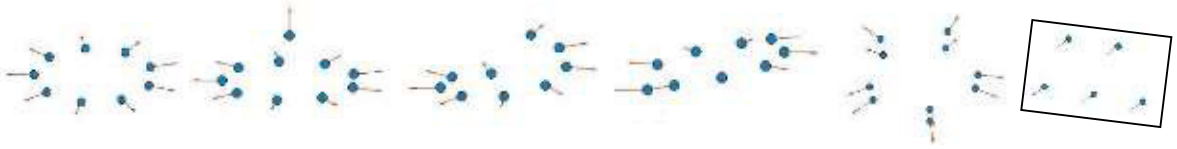

(a) Circular (b) Pyramid (c) Spiral-Circular (d) Slant-Circular (f) Dual-Circular (e) Planar

Fig. 1. The proposal of different array geometries for the DF problem.

3.2. Array Elements

Regardless of DOA estimation algorithm, the choice of elements is indispensable to a DF system functionality. As for what is required for ESM application, the elements must provide the required angular range, dual polarization feature, and frequency bandwidth. To this end, Vivaldi antenna [17, 18] is preferred. This element is a high-gain, light weight, slot-line Ultra Wide Band (UWB), and linearly polarized antenna which has an acceptable VSWR characteristic over a wide band, the main reason why it is applied to this application. However, in order to meet the requirement of no blind polarization against all types of signals, the antenna must radiate at a 45^{o} slant polarization to maximize the received power [1]. Following [17, 18], Vivaldi antenna is designed to radiate at 1 to 2 GHz. Fig.2 illustrates the radiation pattern of the slanted Vivaldi antenna at 1GHz, simulated by using CST Microwave Studio.

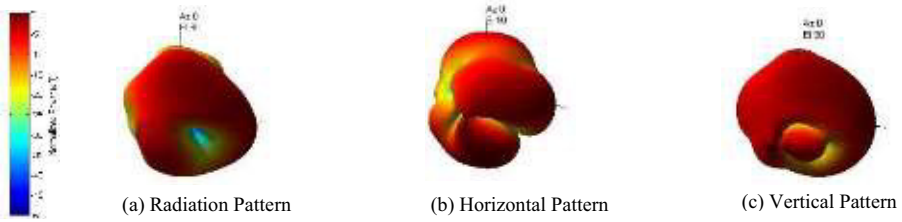

(a) Radiation Pattern (b) Horizontal Pattern (c) Vertical Pattern

Fig. 2. A single slanted Vivaldi radiation patterns at 1GHz

In all the aforementioned geometries, Vivaldi elements are employed apart from the pyramid geometry in which a Monopole antenna is positioned as the center element. Although Monopoles are single polarized antennas [16], they have an omnidirectional radiation pattern which is pertinent for the center element position in the pyramid geometry. Monopoles' impedance is highly sensitive with respect to frequency; therefore, a Sleeve Monopole is designed to increase the bandwidth and adjust input impedance (see [19] and [20] for a discussion in this topic). The antenna was simulated in CST Microwave Studio and transferred to MATLAB for further analysis. The radiation patterns of Monopole are shown in Fig.3.

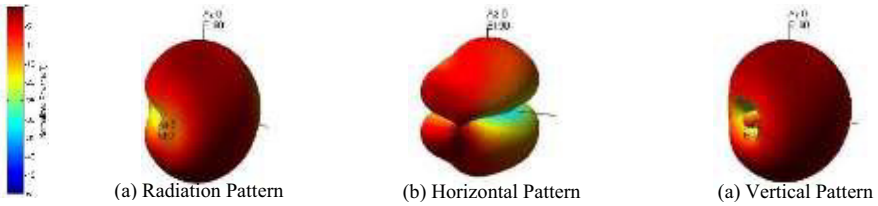

(a) Radiation Pattern (b) Horizontal Pattern (a) Vertical Pattern

Fig. 3. A single Monopole radiation patterns at 1GHz

4. Geometries' Appraisal

4.1. Cramer-Rao Bounds

In this section, in order to evaluate the performance of the proposed array geometries independently of DOA estimation algorithms, the well-known Cramer-Rao bounds (CRBs) of each geometry is investigated. The CRB is a parametric measure of performance which indicates the lower bound on the variance of any unbiased estimator [5, 15]. For an array geometry having elements located in R^3 and an incident signal from the direction of (φ, θ), where the $\varphi \in [0,2\pi)$ and $\theta \in (-\pi/2, \pi/2)$ illustrate its azimuth and the elevation, the single source CRB is given by [15]:

$$CRB(\varphi,\theta) = [G(B,\varphi,\theta).P]^{-1} \tag{3}$$

In (3), the CRB is comprised of two terms. The first term $G(B,\varphi,\theta)$ is based on the source DOA and the array geometry parameter through the matrix B and is given by (4) to (7), and (6); the second term (P), given by (8), is controlled by source and noise powers as well as the operating frequency. In other words, regardless of being narrowband or wideband for a source, and also regardless of the receiving SNR, the impact of a particular geometry on the CRB is the same, thereby providing an important property to compare the geometries [15].

$$G(B,\varphi,\theta) = J_{\varphi,\theta}(u)^T B J_{\varphi,\theta}(u) \tag{4}$$

$$J_{\varphi,\theta}(u) = \begin{bmatrix} \sin\theta\sin\varphi & -\cos\theta\cos\varphi \\ \sin\theta\cos\varphi & \cos\theta\sin\varphi \\ 0 & \sin\theta \end{bmatrix} \tag{5}$$

$$B = \frac{1}{N}\sum_{m=1}^{N}(l_m - l_c)(l_m - l_c)^T \tag{6}$$

$$l_c = \frac{1}{N}\sum_{m=1}^{N} l_m \tag{7}$$

$$P = \frac{2K(2\pi N/\lambda)^2.SNR^2}{1+SNR.N} \tag{8}$$

where N denotes the number of elements, $l_m = [x_m, y_m, z_m]$, $m=1,\ldots,N$ is the position vector of *mth* element in R^3, K is the number of snapshots, λ demonstrates the wavelength, l_c denotes the array geometric center, and $J_{\varphi,\theta}(u)$ is the 3×2 Jacobian matrix of incident angles.

The CRB of the proposed geometries, simulated for *SNR=10dB*, *K=600* samples, is demonstrated in Fig.4. The simulation can be assessed separately for the azimuth angles by CRB_φ, and for the elevation angles by CRB_θ. However, since our simulations illustrate that in the azimuth angle ranges for almost all proposed geometries, the CRB_φ is not affected in our elevation angular range, namely 0 to 60 degrees, and also since the elevation angle estimation is more of a concern in our application, the analysis of CRB_θ is provided herein.

From Fig. 4, we observe that for UCA geometry, when the elevation angle is close to 0 degree, the CRB of the

elevation angle is relatively poor that is in UCA geometry the elevation angle estimation accuracy degrades when the waveforms arrive are travelling from the horizon. Furthermore, according to the Fig. 4, apart from the planar geometry, the CRB of the elevation angle for the other geometries has not asymptotic features any more, which means an improvement for the performance of the elevation angle estimations. The slant and spiral geometries, having two peaks in two special angles, do not suffer from near-zero-elevation accuracy. As for planar geometry, at the elevation angle of 90 degree, the normal of the array, the best accuracy is attained, whereas with receding into the edge of the plane the accuracy degrades.

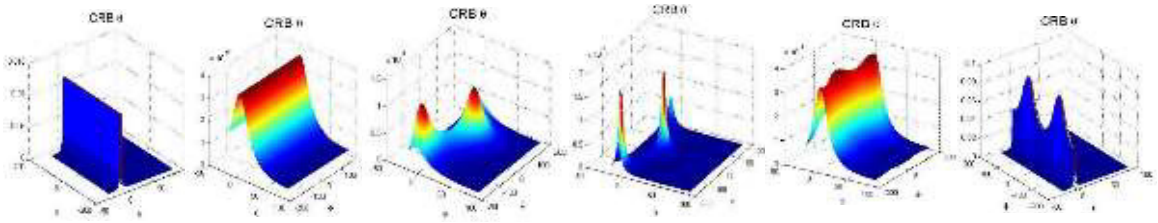

(a) Circular (b) Pyramid (c) Slant (d) Spiral (e) Dual-Circular (f) Planar

Fig. 4. The elevation angle CRB of different geometries

4.2. Ambiguities

Ambiguity problem of the proposed array geometries is considered in this section. Super-resolution algorithms such as MUSIC assume that the array manifold, completely characterizing the array geometry, is known (theoretically or by calibration). However, in the case of one incident signal, when the array manifold of two distinct DOAs equals, $a(\varphi_i,\theta_i)=a(\varphi_j,\theta_j), i\neq j$, then *Ambiguity I* occurs (see [11] for a discussion on this topic). To evaluate Ambiguity I of the proposed geometries, the following function is used [11]:

$$\mathrm{X}_{ij}^{I}(\varphi_i,\theta_i,\varphi_j,\theta_j)=\frac{a(\varphi_i,\theta_i)^{*}a(\varphi_j,\theta_j)}{\left\|a(\varphi_i,\theta_i)\right\|\left\|a(\varphi_j,\theta_j)\right\|} \tag{9}$$

Where * stands for conjugate transposition and $\|.\|$ indicates Euclidian norm of the vector. The Ambiguity I function in (9) ranges from 0 to 1, corresponding to perfect orthogonality or correlation.

Fig.5 shows the ambiguity functions of the proposed geometries. Since in a practical ESM environment most of the targets are identified near the horizon, the ambiguity functions' comparison is carried out at the elevation angle of 0 degree. The best ambiguity performance has the correlation of array manifold of two distinct DOAs as small as possible. Having a decent ambiguity pattern for a geometry, the super-resolution algorithms can solve the incident signal's DOA. All the geometries which are derived from the circular array –namely circular, pyramid, slant, spiral, and dual-circular geometries –manifest a diagonal-like pattern meaning there is almost no ambiguity in azimuth plane. The planar geometry ambiguity function nevertheless, is fully or partially correlated with some other DOA when signals are coming from the array end-fire i.e. away from the array normal.

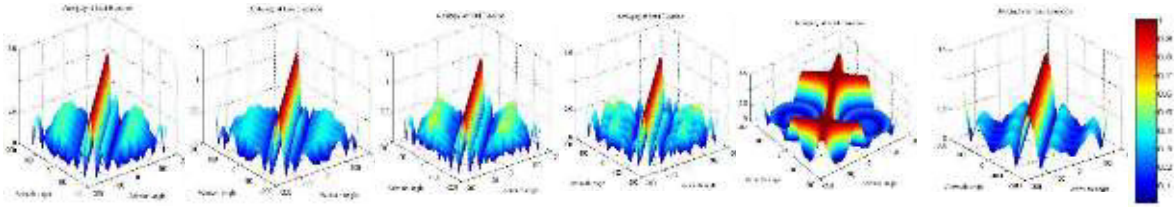

(a) Circular (b) Pyramid (c) Slant (d) Spiral (e) Planar (f) Dual-Circular

Fig. 5. Ambiguity I function of proposed geometries.

5. Simulation Results

In the following, the performance of DOA estimation for suggested geometries employing MUSIC is investigated. Root Mean Square Error (RMSE) criterion [3, 4] is used to compare the accuracy of the estimation in the different array geometries. In the simulation the SNR is set to 10dBm, the number of snapshots is K=600, and 20 independent runs is used to compute RMSE of azimuth and elevation angle estimations for each geometry. Fig. 6 compares the results between presented geometries. In this simulation RMSE of the azimuth estimation, elevation estimation, and the joint RMSE using (10) are studied, but only the results of the joint RMSE are shown; other results are compared in Table1.

$$RMSE_{total} = \sqrt{E[(\hat{\theta}_i - \theta_i)^2 + (\hat{\varphi}_i - \varphi_i)^2]} \tag{10}$$

where E is the expectation of estimated angles, $\hat{\theta}_i$ and $\hat{\varphi}_i$ show the estimated elevation and azimuth angle of the *ith* element, $i=1,\ldots, N$, respectively.

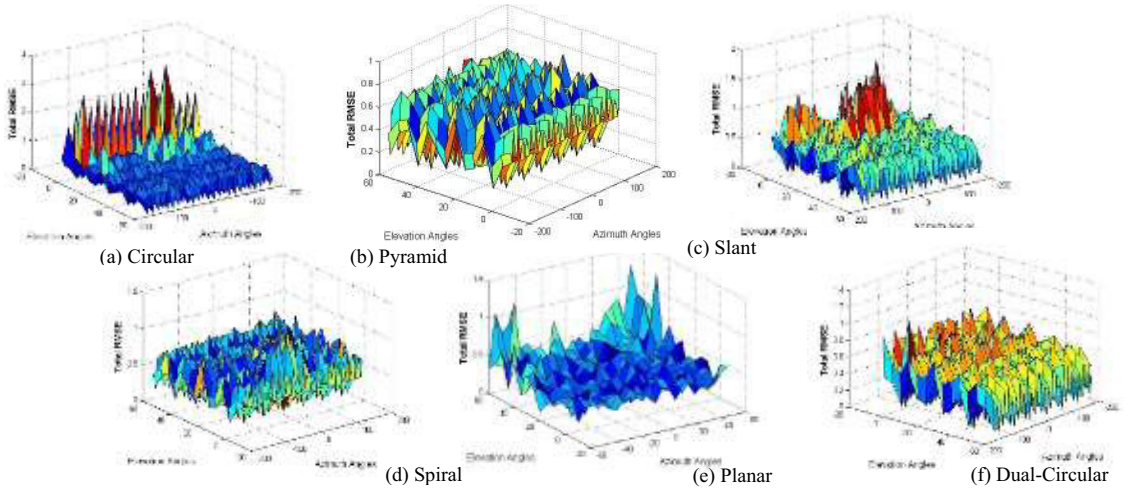

(a) Circular (b) Pyramid (c) Slant

(d) Spiral (e) Planar (f) Dual-Circular

Fig. 6. The Joint RMSE of proposed geometries.

TABLE 1. COMPARISON OF GEOMETRIES PERFORMANCE

Geometry	Azimuth RMSE Average	Elevation RMSE Average	Max. Azimuth Error	Max. Elevation Error	Max. Ambiguity
Circular	0.1170	0.1140	0.4125	0.8361	0.4963
Pyramid	0.1184	0.1098	0.5615	0.3613	0.4191
Slant	0.1206	0.1869	0.6609	2.192	0.5881
Spiral	0.1229	0.1855	0.5674	1.152	0.5769
Dual-Circular	0.1154	0.1231	0.4125	1.133	0.3748
Planar	0.1359	0.0560	3.522	0.3533	1

It is evident from Fig.6 that circular and slant geometries have some difficulties in DOA estimation for near-the-horizon targets, as it was expected from previous CRBs' comparison results. Other full-channel geometries improve the results in term of the foregoing property; however, some geometries such as spiral and dual-circular geometries have bigger maximum elevation error than pyramid and circular geometries. On the other hand, by virtue of using larger number of elements, planar geometry has the best accuracy; nonetheless, the angular field of view must be

confined to ±70 degrees in order to accurately calculate the estimations. It is important to note that the planar geometry is a switching-channel geometry and needs different hardware to be implement. Considering above analysis and results, for full-channel geometries, the dual-circular geometry has an acceptable ambiguity performance that is the lowest amount of correlation in angular field of view, and the pyramid geometry has a satisfactory performance in terms of accuracy.

6. Conclusion

In this work, the analysis and comparison of different array geometries for 2D direction finding, utilizing MUSIC algorithm, as a part of ESM system are carried out. We have studied the limitations of the geometries, and adopted different criteria such as CRBs, ambiguity functions, and RMSEs to compare the geometries. The phase and amplitude characteristics of the antenna elements, namely Vivaldi and Monopole antenna, are especially integrated to the simulations to attain a more accurate model. It has been shown that all the proposed geometry have fitting performance for ESM application. However, the accuracy of the estimations reaches its peak by using pyramid or planar geometries. Moreover, the acme of ambiguity performance is obtained by using dual-circular geometry.

References

1. Martino A. de. *Introduction to Modern EW Systems*. Arthech House, 2012.
2. Schmidt R.O. *Multiple emitter location and signal parameter estimation*. IEEE Trans. Antennas Propag. 34 (3) (1986) 276–280.
3. Khallaayoun A. *High Resolution Direction of Arrival Estimation Analysis and Implementation in a Smart Antenna System*. Doctor of Philosophy dissertation, Montana State University, May 2010.
4. Xiong H. *Antenna array geometries and algorithms for direction of arrival estimation*. MRes thesis, University of Nottingham, 2013.
5. Manikas A., Alexiou A.and Karimi H. *Comparison of the Ultimate Direction-finding Capabilities of a Number of Planar Array Geometries.* IEE Proc. Radar, Sonar, Navig., vol. 144, No. 6, pp. 321-329, 1997.
6. Mahmoud K. R., El-Adawy M., Ibrahem S. M. M., Bansal R., and Zainud-Deen S. H. *A comparison between circular and hexagonal array geometries for smart antenna systems using particle swarm optimization algorithm.* Progress in Electromagnetics Research, vol. 72, pp. 75–90, 2007.
7. Tan C. M., Fletcher A., Beach M. A., Nix A. R., Landmann M., and Thoma R. S. *On the application of circular arrays in direction finding, Part I: Investigation into the estimation algorithms*. IEEE 1st Workshop on Opportunities of the Multidimensional Propagation Channel, 29-30, 2002.
8. Tan C. M., Fletcher A., Beach M. A., Nix A. R., Landmann M., and Thoma R. S. *On the application of circular arrays in direction finding, Part II: Experimental evaluation on SAGE with different circular arrays.* IEEE 1st Workshop on Opportunities of the Multidimensional Propagation Channel, 29-30, 2002.
9. . Poisel R. A. *Antenna Systems and Electronic Warfare Application*. Norwood, MA, Artech House, 2011.
10. Rancy F. *ITU-R Spectrum Monitoring Handbook.* 1st ed; Geneva, Switzerland, 2011.
11. Eric M., Zejak A., Obradovic M. *Ambiguity characterization of arbitrary antenna array: type I ambiguity.* Proceedings of IEEE International Symposium on Spread Spectrum Techniques and Applications, 2-4 Sep. 1998, pp 399-403.
12. Azremi A.A.H., Costa M., Koivunen V. and Vainikainen P. *Ambiguity analysis of isolation-based multi-antenna structures on mobile terminal," In Proceedings of the 5th European Conference on Antennas and Propagation*. 11-15 April, 2011, Rome, Italy, pp. 552-556
13. Josefsson L. and Persson P. *Conformal array antenna theory and design.* John Wiley & Sons, Inc., New Jersey, 2006.
14. Manikas A., Sleiman A., Dacos Z. *Manifold Studies of Nonlinear Antenna Array Geometries*. IEEE Transactions on Signal Processing, vol.49, pp.497-506, March 2001.
15. Baysal U. and Moses R. L. *On the Geometry of Isotropic Arrays," IEEE Trans. On Signal Processing*. vol. 51, no. 6, pp. 1469-1478, June 2003.
16. Balanis C. *Antenna Theory: Analysis and Design*. 2nd ed. John Wiley & Sons, May 1996.
17. Ying Li, Chen Ai-xin. *Design and application of Vivaldi antenna array*. Antennas, Propagation and EM Theory, 2008. ISAPE 2008. 8th International Symposium on , vol., no., pp.267-270, 2-5 Nov. 2008.
18. Xu H., Zhao G., Zhang Z., Sun H., and Lv X. *Antipodal Vivaldi antenna for phased array antenna applications*. 5th Global Symposium on Millimeter Waves (GSMM), 2012, pp. 200-203.
19. Nikolova N. K. *Lecture 11: Practical Dipole/Monopole Geometries Matching Techniques for Dipole/Monopole Feeds*. McMaster University, 2003.
20. Nikolova N. K. *Lecture 10: Other Practical Dipole/Monopole Geometries Matching Techniques for Dipole/Monopole Feeds*. McMaster University, 2003.